Scientia Iranica (2024) 31(13), 1030–1042

Sharif University of Technology
Scientia Iranica
Transactions B: Mechanical Engineering
https://scientiairanica.sharif.edu

A novel method (a tube with successive increase and reduction in diameter) to increase nanofluid heat transfer in a tube

Ahmad Bedram*

Department of Mechanical Engineering, Technical and Vocational University (TVU), Tehran, Iran.

Received 28 June 2022; received in revised form 8 January 2023; accepted 30 May 2023

KEYWORDS
Heat transfer enhancement;
Tube;
Diameter change;
Numerical simulation;
Nanofluid;
Aluminum oxide.

Abstract. A new geometry has been proposed to increase heat transfer in tubes. This geometry has two phases of increase in diameter and a phase of reduction in diameter with two obstacles. The fluid used was water-aluminum oxide (Al_2O_3) nanofluid. Reynolds numbers (Re) of 2-3-00 and nanoparticle volume fraction of 0–3.5% have been investigated. Profile of temperature, velocity and pressure has been presented for different Reynolds numbers, nanofluid volume fractions and sections of geometry. In addition, variations of Nusselt number in different Reynolds numbers and volume fractions have been studied. For different Reynolds numbers, "the increase in heat transfer" and "the reduction in pressure drop" of the proposed geometry compared to a simple tube have been presented. For $Re = 50$, increasing the temperature of the fluid of the geometry proposed in this study was 52% higher than that of a simple tube under the same operating conditions. For the $Re = 50$, the pressure drop of the geometry proposed in this study was 24% less than that of a simple tube under the same operating conditions. The results showed that average Nusselt number in the volume fraction of 3.5% was about 4% higher than the average Nusselt number in the volume fraction of 0.5%.

1. Introduction

Increasing heat transfer in industrial processes is one of the most important topics in various industries. Some applications of this issue are heat transfer increase in evaporators, increased heat transfer in heat exchangers, increased heat transfer using surface roughness adjustment, heat transfer in solar water heaters and heat transfer in closed chambers [1].

There are many methods to increase heat transfer through a channel. One of these methods is to add a twisted tape into the channel [2]. In another method, the tube is made in a wavy or sinusoidal manner

*. *Tel.: +985632838274*
E-mail address: abedram@tvu.ac.ir (A. Bedram)

To cite this article:
Ahmad Bedram "A novel method (a tube with successive increase and reduction in diameter) to increase nanofluid heat transfer in a tube", *Scientia Iranica* (2024), **31**(13), pp. 1030-1042
https://doi.org/10.24200/sci.2023.60676.6935

and heat transfer is increased by forming vorticity in the flow [3]. In another method, obstacles of various shapes are placed in the flow path and heat transfer is increased due to turbulence in the flow [4]. In some methods, heat transfer is increased by adding nanoparticles of a metal to the water flow inside the channel [5].

Masoumnezhad et al. [6] investigated the unstable heat transfer between two oscillating plates under the influence of a magnetic field. Their results showed that by increasing the magnetism quantity, heat transfer rate in the wall increased.

In a review paper, Mousa et al. [7] discussed methods for increasing heat transfer in a single-phase flow. Many methods they have explored are based on adding obstacles of different shapes into the channel.

Khetib et al. [8] investigated heat transfer in a channel with a rectangular cross-section with circular cylinders in its middle. The research method was numerical simulation. They found that $B = 0.5$ T had the highest heat transfer compared to other magnetic fields.

Kia et al. [9] investigated the heat transfer and pressure drop of nanofluid flow in a helical tube. They considered constant heat fluxes boundary condition. Their results revealed the Al_2O_3 nanofluid increased the heat transfer coefficient more than the SiO_2 nanofluid. Also, the helical tube heat transfer is 19.5% more than the straight tube.

Akbarzadeh and Valipour [10] investigated the improvement of heat transfer using helically corrugated tubes. Their results showed that using corrugated tubes increased heat transfer by 85–107% and the coefficient of friction by 25–85%.

Nguyen et al. [11] investigated the effect of adding a triangular obstacle in the flow path on heat transfer through a tube. They also investigated the effect of a magnetic field on the flow. The research method was numerical simulation. The results showed that adding a triangular obstacle increased heat transfer, but in high Reynolds numbers (Re), triangular obstacles caused vortex within the flow.

Pahlevaninejad et al. [12] investigated heat transfer in a wavy tube with square obstacles. The research method was numerical simulation and they used water-Al_2O_3 nanofluid. Their results showed that by increasing the volume fraction of nanoparticles, heat transfer increased. Also the maximum coefficient of friction related to the square obstacle with maximum height.

Rahmati and Derikvand [13] investigated the nanofluid flow in a channel along the porous rectangular obstacles with the slip boundary condition. The research method was numerical simulation using a SIMPLE algorithm. They found that by reducing the Darcy number and porosity, the friction entropy production rate increased by more than 800%.

Abdelmalek et al. [14] investigated fluid flow and heat transfer in a porous channel with triangle, circle and rectangle sections. The research method was numerical simulation and they investigated water-Al_2O_3 nanofluids. The results showed that in different states, by increasing the Reynolds number (Re), the average Nusselt number increased and the friction coefficient reduced.

Miansari et al. [15] investigated the flow of non-Newtonian nanofluid and heat transfer in a rectangular cross-section micro channel. They investigated the effect of the channel height and Reynolds number on temperature profile, pressure drop and Nusselt number. The results showed that increasing the Reynolds number and the height of the channel increased the pressure drop along the channel.

Cheng et al. [16] investigated the heat transfer of hydrocarbon fuel in transverse corrugated tubes under supercritical pressures. Their experimental results showed the concave corrugation enhance the heat transfer by generation of secondary flow and backflow. Their results showed the heat transfer coefficient of the helical tube is 35–51% more than that of the plain tube.

Zhang et al. [17] used a new geometry to increase heat transfer. In their geometry, fins mounted on a tube were used to produce a vortex and increase turbulence. The results showed that their proposed method could increase heat transfer coefficient by 46% compared to geometries without producing vortexes.

Borah et al. [18] investigated the effect of non-uniform heating on the heat transfer for flow of Al_2O_3-water nanofluid through a channel using numerical simulation. Their results indicated the average Nusselt number decreases with amplitude of heat flux. Also the use of nanofluid can enhance the decrease in heat transfer due to non-uniform heating.

Borah and Peti [19] performed a numerical simulation to investigate the effects of non-uniform heating on the heat transfer characteristics for nanofluid flow through a channel. The results showed the heat transfer is higher for the non-uniform heating relative to uniform heating. Also the impact of asymmetric heating is greater than that of non-uniform heating.

Faizan et al. [20] investigated heat tranasfer enhancement for laminar nanofluid flow through a converging channel using numerical simulation. They considered the ranges $700 < Re < 1650$ and $0\% < \varphi < 4\%$ for Reynolds number and nanofluid volume fraction, respectively. Their results revealed the pressure drop in the converging channel increases with the converging angle. Also the pressure drop increases up to 100% by increase of nanofluid volume fraction from 0% to 4%.

Bhowmick et. al. [21] studied the heat transfer Cu-water nanofluid within a corrugated channel. They investigated different profiles such as triangular, sinusoidal and trapezoidal. Their results showed the

trapezoidal corrugated channel has better heat transfer performance compared to sinusoidal and triangular ones. They defined a performance factor for consideration of heat transfer and pressure drop effects. The performance factor is strongly dependent upon the Reynolds number and the profile of the corrugated channel.

Mehta and Pati [22] investigated MWCNT-Fe_3O_4/H_2O hybrid nanofluid flow through a wavy channel under the influence of a magnetic field. Their results showed the value of Nusselt number increases with the increase in nanofluid volume fraction and Hartman number. Also for intermediate range of Reynolds number, magnetic performance factor increases with Hartman number.

Faizan et al. [23] numerically investigated the effect of non-uniform heating of Al_2O_3-water nanofluid flow in a converging channel. Their results indicated enhancement of Nusselt number with the increase in the thermal conductivity of wall and Re number. Also the heat transfer of non-uniform heating case is lower than the constant heat flux one.

In the previous studies, various methods have been used to increase the heat transfer of the nanofluid inside the channel. Also, a significant number of these methods have been mentioned. Most of the methods proposed to increase the heat transfer of the nanofluid inside the channel, in addition to increasing the heat transfer, raise the pressure drop of the system. Given that the pressure drop can increase the cost of system, it is necessary to propose methods that cause less pressure drop. In this paper, a method has been proposed to reduce the pressure drop of the system for small and medium Reynolds numbers, while increasing the heat transfer. The new proposed in this study is presented for the first time.

In this paper, a new geometry has been proposed to increase heat transfer through a tube. This geometry has two phases of increase in diameter and a phase of reduction in diameter with two obstacles in the flow. Al_2O_3 nanoparticles have been used in a large number of studies related to nanofluids [4,5,8,12,14,24,25] with various industrial applications. Therefore, in the present study, water-aluminum oxide (Al_2O_3) nanofluid has been investigated. The results showed that the proposed geometry in this study (compared to a simple tube), in addition to increasing the heat transfer, reduced the flow pressure drop. However, many previous methods that have been proposed to increase heat transfer in tubes also raise heat transfer and pressure drop simultaneously. Numerical results have been validated by comparing the results with the experimental ones. Also, the grid independency was done. The Reynolds numbers of 2–300 and the nanoparticle volume fraction of 0–3.5% were investigated. Profile of temperature, velocity and pressure was presented for different Reynolds numbers, nanofluid volume fractions and sections of geometry. Changes in the Nusselt number, Reynolds numbers and volume fractions were presented. For different Reynolds numbers, the increase of heat transfer and the reduction in the pressure drop of the proposed geometry were compared to those of the simple tube.

2. Geometry

The proposed geometry of this paper is shown in Figure 1. As can be seen, the fluid enters through a tube with a diameter of 90 micrometers and finally exits through a tube with a diameter of 90 micrometers. In the middle of the tube, there is an expansion so that the diameter of the tube reaches to about 240 micrometers. When the diameter of the tube is increased, there are two obstacles (with the height of 60 and 120 micrometers).

As shown in Figure 1, the geometry diameter increases between A and B. In this area, the angle of the tube wall (θ_1) is 26.6 degrees. At point B, there is an obstacle with the height of 60 micrometers in the middle of the channel. Also, the diameter of geometry increases between B and C. In this area, the angle of the tube wall (θ_2) is equal to 18.4 degrees. At point C, there is an obstacle with the height of 120 micrometers in the middle of the channel. The reason for the increase of channel diameter in areas between points A to C is reducing the pressure drop of the system. To explain, if the outer diameter of the channel is constant and the channel has some obstacles, the pressure drop will increase significantly. The diameter of the channel is fixed between C and D. The diameter of the channel is reduced between D and E. In this area, the angle of the tube wall (θ_3) is 39.8 degrees. θ_1, θ_2, and θ_3 are selected in such a way that the cross-section area of the fluid is not less than that of the input tube.

The fluid passing through the tube is water-aluminum oxide nanofluid. The following equations can be used to calculate the nanofluid properties [24]:

$$\rho_{nf} = \varphi\rho_p + (1-\varphi)\,\rho_{bf}, \tag{1}$$

$$\frac{k_{nf}}{k_{bf}} = 4.97\varphi^2 + 2.72\varphi + 1, \tag{2}$$

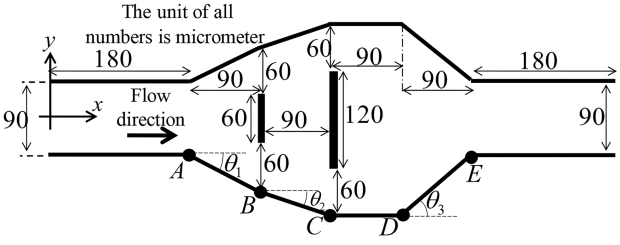

Figure 1. Problem geometry; The nanofluid flow enters from the left and exits from the right.

Table 1. Physical properties of the fluids [24,25].

Fluid	Density (kg/m^3)	Conductivity (W/mK)	Specific heat capacity (J/kgK)	Viscosity (kg/ms)
Water	997	0.606	4179	0.00089
Al_2O_3	3970	40	765	–
Nanofluid 3%	1086.32	0.6582	3804.687	0.0011834

Table 2. Geometrical parameters of the system.

Parameter	Value (μm)	Parameter	Value (μm)
Inlet diameter	90	First obstacle height	60
Outlet diameter	90	Second obstacle height	120
Maximmun diameter	240	Horizontal distance between two obstacles	90
System length	720		

$$\frac{\mu_{nf}}{\mu_{bf}} = 123\varphi^2 + 7.3\varphi + 1, \tag{3}$$

$$c_{nf} = \frac{\varphi\rho_p c_p + (1-\varphi)\,\rho_{bf} c_{bf}}{\rho_{nf}}, \tag{4}$$

where φ is the volume fraction of nanoparticles in the base fluid, k is the thermal conductivity, ρ is the density, μ is dynamic viscosity, c is the specific heat capacity, and nf, bf, and p indicate nanofluid, base fluid and nanoparticles, respectively. Table 1 shows the properties of water and aluminum oxide (Al_2O_3). Using Eq. (1) and Table 1, the nanofluid properties can be obtained in any given percentage of nanoparticles. For example, properties of 3% volume fraction nanofluid are presented in the Table 1.

The Reynolds number of nanofluid is defined as follows [26]:

$$Re_{nf} = \frac{\rho_{nf}\bar{U}D}{\mu_{nf}}, \tag{5}$$

where ρ and μ are density and viscosity, respectively, and nf indicates nanofluid. D is the diameter of the channel and $\bar{U}$ is the average velocity of the fluid in the channel.

In the diverging-converging section of the geometry, the cross-section area is variable. Therefore, it is not possible to define a specific value for the hydraulic diameter. In other words, if we want to define a hydraulic diameter for the divergent-convergent tube, each of the sections will have a unique hydraulic diameter. Therefore, in this paper, we consider the hydraulic diameter to be the same as the diameter of the tube at point A (Figure 1).

Tang et al. [27] stated "Inertial microfluidics works in an intermediate Reynolds number range ($\sim 1 < Re <\sim 100$)". In this paper, $2 < Re < 300$ is considered for Reynolds number range.

The Nusselt number is defined as follows:

$$Nu = \frac{hd}{k_{nf}}, \tag{6}$$

where h is the convection heat transfer coefficient, d is the diameter of the inlet channel, and k_{nf} is the thermal conductivity of the nanofluid.

Table 2 shows the geometrical parameters of the system.

3. Numerical simulation

The flow is steady state, incompressible and the equations of continuity, momentum and energy are as follows [17,28]:

$$\frac{\partial u_i}{\partial x_i} = 0$$

$$\rho\left(\frac{\partial u_i}{\partial t} + u_j\frac{\partial u_i}{\partial x_j}\right) = \rho g_i - \frac{\partial p}{\partial x_i} + \mu\frac{\partial^2 u_i}{\partial x_j^2},$$

$$\frac{\partial\left(u_i T\right)}{\partial x_i} = \frac{k}{\rho c_p}\frac{\partial^2 T}{\partial x_i^2}, \tag{7}$$

where k is the thermal conductivity, ρ is density and c_p is specific heat capacity of the fluid. The numerical simulation was performed using Ansys Fluent v.15. The criteria for completing the numerical solution is that the residuals are smaller than 0.0001.

The geometry of the problem has been presented and meshed by software Gambit. The size of the mesh has been reinforced near the walls. Discretization of momentum and energy equations is established by the second order upwind method and the pressure-velocity coupling is established by the algorithm SIMPLEC. The flow is laminar and the boundary conditions are constant velocity for inlet, constant pressure for outlet and no-slip for walls. Thermal boundary condition for walls is constant heat flux of 10,000 W/m^2.

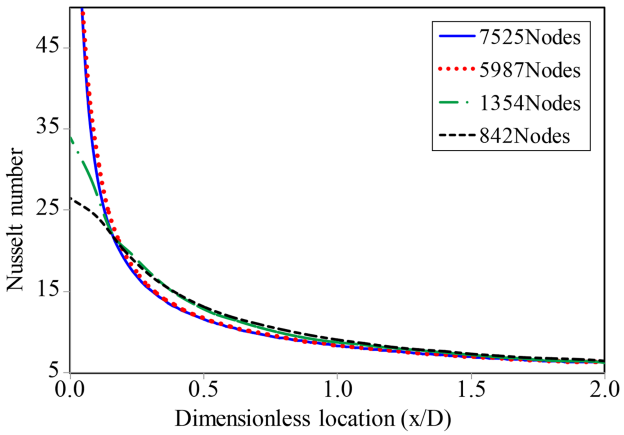

Figure 2. Grid independency for nanofluid of water-Al_2O_3(2%) in four grids of different sizes.

To study grid independency, water-Al_2O_3(2%) nanofluid was considered in the geometry of the problem. The results have been compared in four grids of different sizes. Figure 2 shows the Nusselt number along geometry in four different grids. As shown, for grids with more than 5987 nodes, the results are grid independent.

An experimental study by Kim et al. [29] was used to validate the numerical simulation performed in the paper. In the paper of Kim et al., the flow of water-Al_2O_3(3%) nanofluid in a tube with a diameter of 4.57 mm, length of 2 m and Reynolds number 1460 which has a wall with a constant heat flux is investigated and the heat transfer coefficient along the tube is reported. Figure 3 compares the heat transfer coefficient along the tube derived from numerical simulation of this paper with the experimental results of Kim et al.. As shown, there is a good agreement between the results of the present study and the experimental results of Kim et al.

For validation of pressure drop results, an experimental study by Chandrasekar et al. [30] was used. In the paper of Chandrasekar et al., the flow of water-Al_2O_3(0.1%) nanofluid in a tube with a diameter of 4.58 mm and length of 1.2 m which has a wall with a constant heat flux is investigated and the friction factor is reported. Friction factor defined as $f = \Delta P/(0.5\rho V^2 L/D)$ that ΔP is the pressure drop, ρ is the nanofluid density, V is the fluid velocity magnitude, L and D are length and diameter of the tube, respectively. Figure 3(b) compares the friction factor derived from numerical simulation of this paper with the experimental results of Chandrasekar et al.. As shown, there is a good agreement between the results of the present study and the experimental results.

4. Results and discussion

Figure 4 shows a three-dimensional view of the geometry of the problem. The flow enters the geometry from

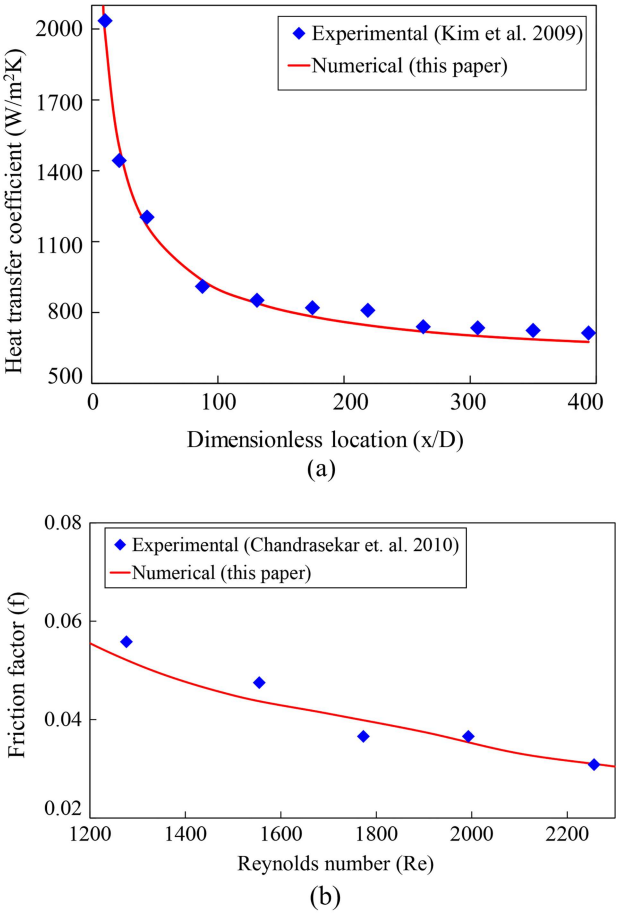

Figure 3. Validation of numerical simulation. (a) The heat transfer coefficient validation. (b) The pressure drop validation.

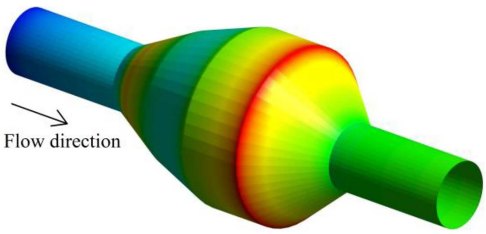

Figure 4. Three-dimesional view of the problem geometry.

the left and exits from the right. First, the diameter of the tube increases and then suddenly reduces. The diameter of the inlet and outlet of the system is the same.

Figure 5(a) shows the streamlines and Figure 5(b) shows velocity magnitude contour of the nanofluid flow of water-Al_2O_3(2%) and the Reynolds number 200. As shown, the nanofluid flows from left to right, and when it reaches the first obstacle, the flow separates from the obstacle. After the first obstacle (between the two obstacles), two large vortexes are formed. At the location of the first obstacle, the diameter of the channel is also increased. This means that neither

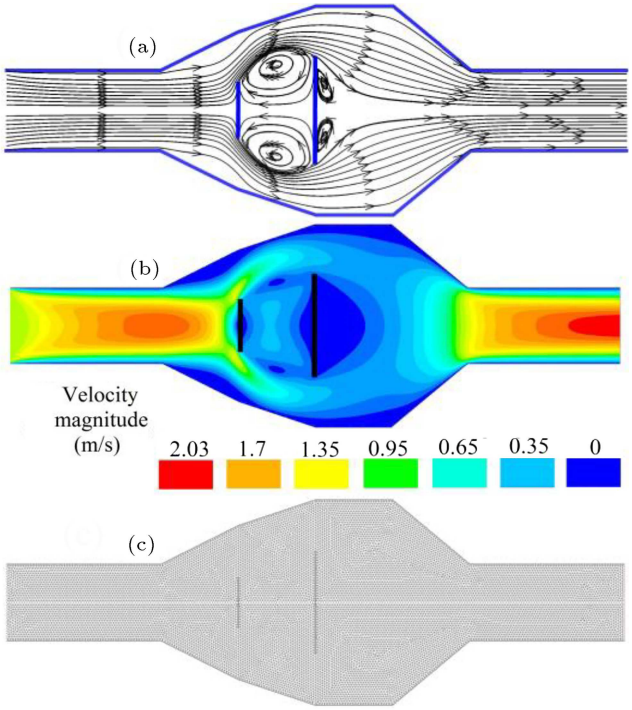

Figure 5. (a) Streamlines; (b) Velocity magnitude contour of water-Al_2O_3(2%) nanofluid for the Reynolds number 200; (c) Considered mesh for simulation. The mesh is adapted near the walls.

the presence of the first obstacle nor flow separation at the location of the first obstacle can increase the velocity of the fluid. Therefore, it is observed that the fluid velocity at the location of the first obstacle (and slightly before and after it) is almost the same; even when the flow reaches the second obstacle, the flow velocity is reduced, which can be regarded as one of the advantages of the proposed geometry. There is a slight pressure drop in this geometry, detailed diagrams of which are illustrated in the next figures. Also Figure 5(c) shows the considered mesh for simulation. The mesh is adapted near the walls.

To present the results of numerical simulation, eight vertical sections in several locations of the problem geometry are considered. These eight sections are shown in Figure 6. The dimensionless location is defined by the following equation and the location of each section is determined by this:

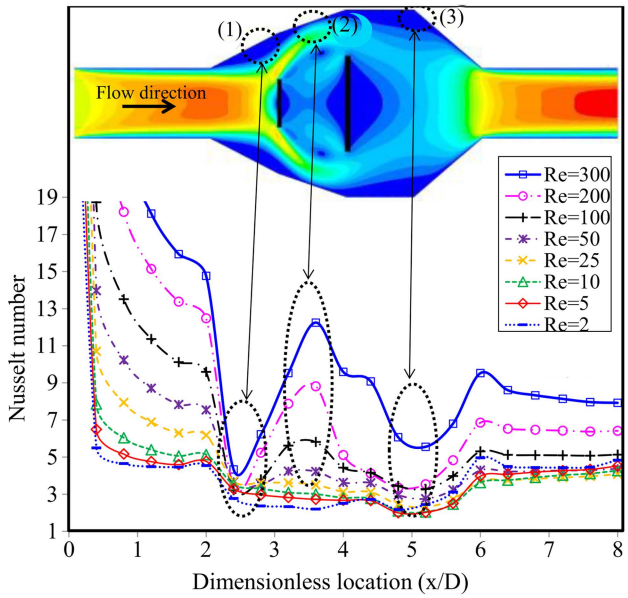

Figure 7. Nusselt number of water-Al_2O_3(2%) nanofluid along the channel with different Reynolds numbers. The dimensionless location is defined by Eq. (8). The velocity magnitude contour of the fluid is also shown in the figure.

$$\text{Dimensionless location} = \frac{x}{D}, \tag{8}$$

where x is the distance of the given section to the system inlet and D is the diameter of the input channel.

Figure 6 shows fluid pressure for water-Al_2O_3(2%) nanofluid for the Reynolds number of 200. As shown, the average pressure of the fluid between $x/D = 0.8$ and $x/D = 5.6$ is between 6000 Pa and 7200 Pa, with a slight change.

Figure 7 shows the Nusselt number of water-Al_2O_3(2%) nanofluid along the channel for different Reynolds numbers. The dimensionless location is

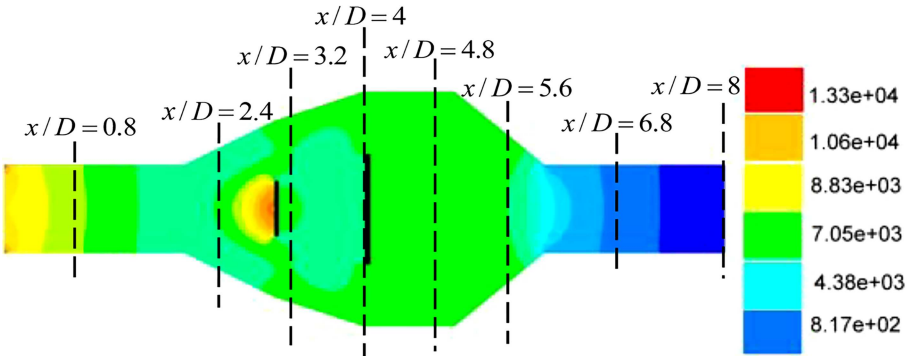

Figure 6. Pressure (in Pascal) of water-Al_2O_3(2%) nanofluid for the Reynolds number 200. In the figure eight different vertical sections have been illustrated. The results presented in the rest of the paper are related to these eight sections.

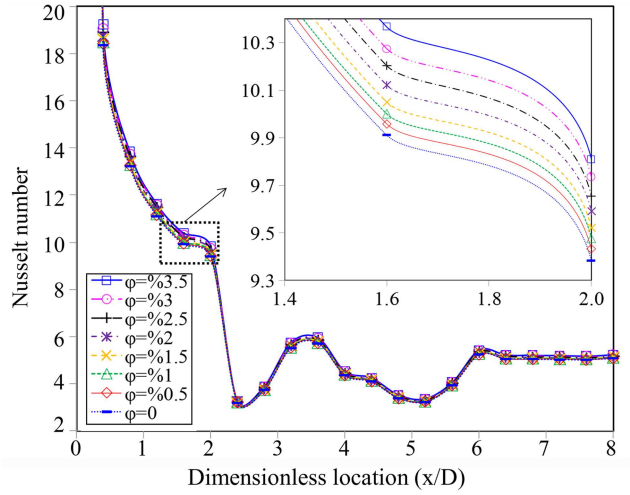

Figure 8. Nusselt number of water-different percentages of Al_2O_3 nanofluid along the tube with the Reynolds number 100. The dimensionless location is defined by Eq. (8).

defined by Eq. (8). The contour of fluid velocity magnitude is also shown in the Figure 7. As shown, for $x/D \approx 2.5$ a sudden reduction was observed in the Nusselt number (especially in larger Reynolds numbers). On the velocity magnitude contour of Figure 7, a location is marked with the number (1), which is $x/D \approx 2.5$. Therefore, the sudden reduction in the Nusselt number for $x/D \approx 2.5$ is due to the fact that the channel diameter increases in this location; then the flow is separated from the upper wall. Therefore, the fluid velocity is reduced in locations close to the wall, thus decreasing the local Nusselt number. Also, As shown, the Nusselt number is raised for $x/D \approx 3.5$. In the velocity magnitude contour shown in Figure 7, $x/D \approx 3.5$ is marked with the number (2). The reason for the increase of the Nusselt number for $x/D \approx 3.5$ is that in this region, due to the flow separation from the smaller obstacle, the fluid velocity near the wall is increased. Also, as shown in Figure 7, for $x/D \approx 5$, the Nusselt number is reduced. In the velocity magnitude contour shown in Figure 7, $x/D \approx 5$ is marked with the number (3). The reason for the reduction in the Nusselt number for $x/D \approx 5$ is that the fluid velocity near the wall is decreased due to the flow direction to the output channel. Also, the Nusselt number is raised with the increase of the Reynolds number. The mean Nusselt number for Reynolds numbers 2, 5, 200, and 300 is 5.25, 5.66, 14.85, and 17.80, respectively. Therefore, by increasing the Reynolds number from 2 to 5 (i.e., double and half of the Reynolds number), the Nusselt number is increased by about 8%. However, by raising the Reynolds number from 200 to 300 (i.e., one and half of the Reynolds number), the Nusselt number is increased by about 20%, thus indicating that the heat transfer can be increased for higher Reynolds numbers.

Figure 8 shows the Nusselt number of nanofluid

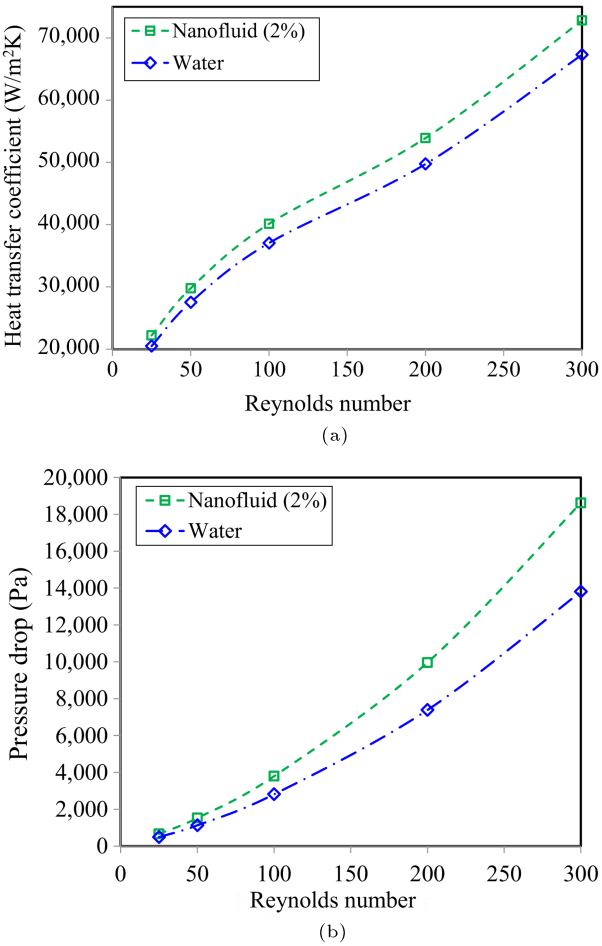

Figure 9. Comparison of heat transfer coefficient and pressure drop of the Nanaofluid (2%) and pure water for different Reynolds numbers.

of water and different percentages of Al_2O_3 along the channel for the Reynolds number 100. Dimensionless location is defined by Eq. (8). As shown, changes in the volume fraction of nanoparticles have little effect on the Nusselt number. For example, the average Nusselt number along the tube is equal to 12.2 for nanofluids with the volume fraction of 3.5% and 11.7 for nanofluids with the volume fraction of 0.5% (a decrease of about 4%).

Figure 9 compares heat transfer coefficient and pressure drop of "2% nanofluid" and "pure water". The results of Figure 9 are related to the fluid flow in the geometry proposed in this study. As shown, the heat transfer coefficient of the nanofluid is higher than that of pure water, and raising the Reynolds number increases such a difference. For example, for the Reynolds number 25, the heat transfer coefficient of nanofluid is 1716 W/m^2K more than that of pure water; at Reynolds number 300, this difference reaches 5488 W/m^2K. Also, the pressure drop of the nanofluid is higher than that of pure water, and raising the Reynolds number increases the difference in the

pressure drop of the nanofluid and pure water. For example, for the Reynolds number 25, the pressure drop of the nanofluid is 171 Pa more than that of pure water, and for the Reynolds number 300, this difference reaches to 691 Pa.

Now, we compare our results with the results of previous studies. For example, in a study by Nguyen et al. [11] several triangular obstacles have been used to increase heat transfer. In this study, the heat transfer coefficient for Reynolds number 5 is equal to 0.87 W/m^{2}K. While in the present study, the heat transfer coefficient for Reynolds number 5 is equal to 1.42 W/m^{2}K.

Pahlevaninejad et al. [12] used a wavy microchannel to increase heat transfer. In this study, for volume fraction of 1.5%, Reynolds number 300 and geometry MC-3, Nusselt number is 9.81 and mean friction coefficient is $C_f = 0.17$. While in the present study, for volume fraction of 1.5% and Reynolds number 300, Nusselt number is equal to 10.16 W/m^{2}K and friction coefficient is equal to $C_f = 0.046$.

Shamsi et al. [4] used a tube with triangular ribs to increase heat transfer. In this study, for volume fraction of 1.5% and Reynolds number of 300, the highest Nusselt number is equal to 7.35 and the mean friction coefficient is equal to $C_f = 0.058$. While in the present study, for volume fraction of 1.5% and Reynolds number 300, the heat transfer coefficient is equal to 10.16 W/m^{2}K and the friction coefficient is equal to $C_f = 0.046$.

Figure 10 shows the streamlines and vortexes for different Reynolds numbers. As shown, for $Re = 5$, two small vortexes are formed after the first obstacle. By increasing Reynolds number, the dimensions of the vortexes become larger. Therefore, two vortexes are formed for $Re = 25$ (but with larger dimensions than $Re = 5$). For $Re = 100$, the dimensions of the vortexes after the first obstacle are increased and two new vortexes are formed after the second obstacle. Figure 10 shows the point A. We draw a tangent line on the vortex from A. The angle of this line with the horizontal direction is called α. By raising the Reynolds number and vortex size, α increases. Increasing α causes the reduction of the available space for the fluid to pass above the first obstacle; as a result, the fluid velocity increases.

Figure 11 shows temperature profile for $x/D = 3.2$ as a function of Reynolds numbers for water-Al_2O_3(2%) nanofluid. As shown, temperature profile for Reynolds numbers less than 10 has a constant value in the central parts of the tube. This constant temperature is at the dimensionless location between -0.45 and 0.45. It is due to the presence of the smaller obstacle in this region of the flow. For low Reynolds numbers, the middle region of the channel, which has a constant temperature, is smaller. For

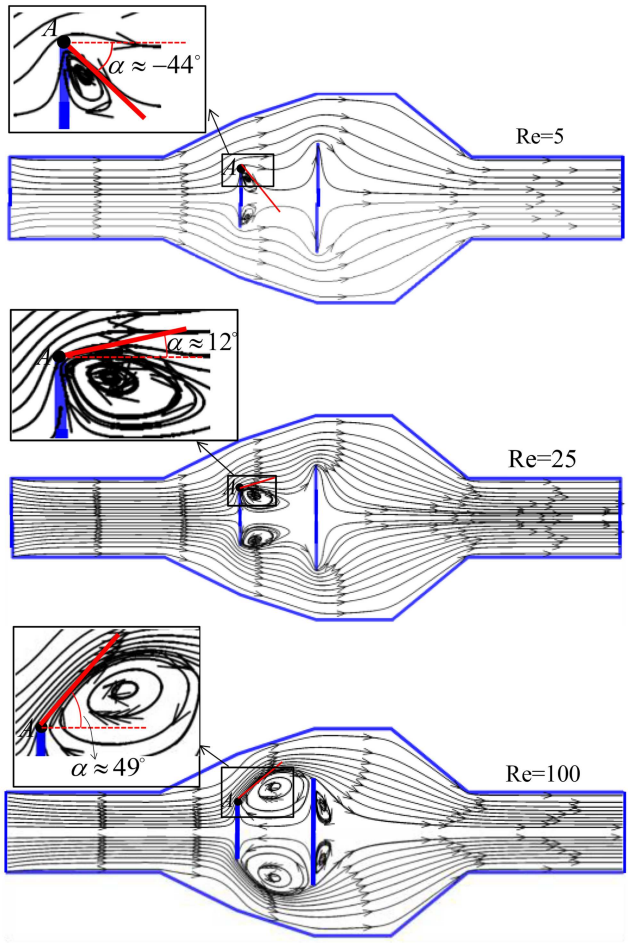

Figure 10. Streamlines and vortexes in the nanofluid flow.

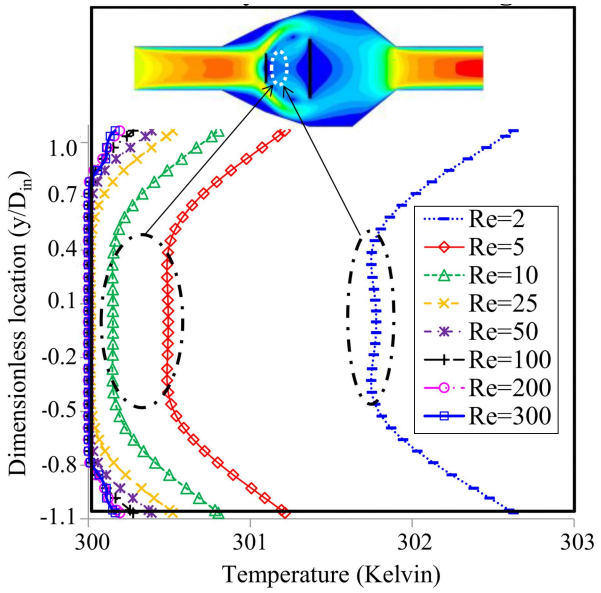

Figure 11. Temperature profile for $x/D = 3.2$ and different Reynolds numbers for water-Al_2O_3(2%) nanofluid. The exact location of the section $x/D = 3.2$ is shown in Figure 6. D_{in} is the diameter of the input channel and the y-axis is shown in Figure 1.

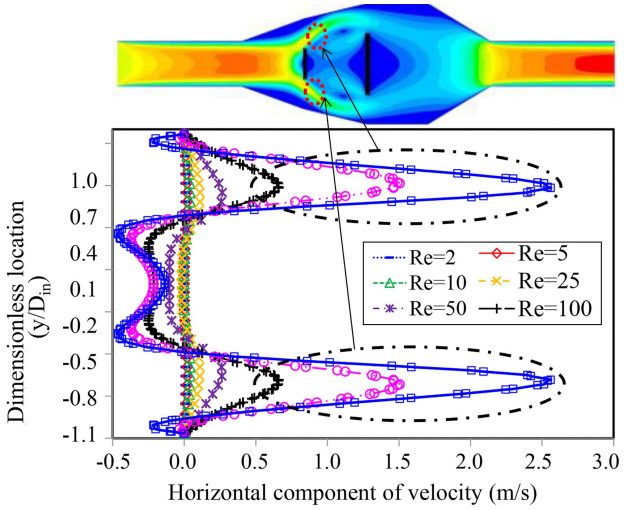

Figure 12. Profile of x-component of velocity for $x/D = 3.2$ as a function of Reynolds numbers for water-Al_2O_3(2%) nanofluid. The exact location of the section $x/D = 3.2$ is shown in Figure 6. D_{in} is the diameter of the input channel and the y-axis is shown in Figure 1.

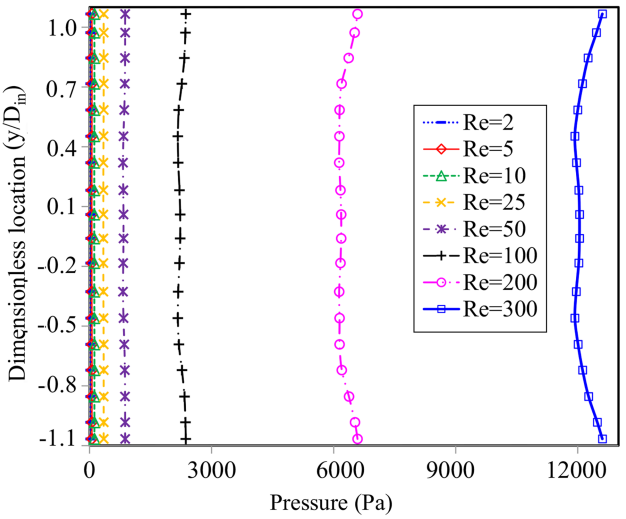

Figure 13. Pressure profile for $x/D = 3.2$ as a function of Reynolds numbers for water-Al_2O_3(2%) nanofluid. The exact location of the section $x/D = 3.2$ is shown in Figure 6. D_{in} is the diameter of the inlet channel and the y-axis is shown in Figure 1.

example, for $Re = 2$, the constant temperature range is $-0.45 < y/D_{in} < 0.45$ and for $Re = 100$, the constant temperature range is $-0.8 < y/D_{in} < 0.8$. The reason is that for low Reynolds numbers, as shown in Figure 10, α is reduced and the effects of temperature changes are transferred to the middle regions of the channel.

Figure 12 shows profile of the x-component of velocity for $x/D = 3.2$ as a function of Reynolds numbers for water-Al_2O_3(2%) nanofluid. The exact location of the section $x/D = 3.2$ is shown in Figure 6. D_{in} is the diameter of the inlet channel and the y-axis is shown in Figure 1. As shown in Figure 12, large vortexes are formed behind the obstacle, and the presence of vortexes could reduce the velocity. Therefore, there is maximum velocity in the upper and lower parts of the obstacle. It could be observed that for almost all Reynolds numbers, in some dimensionless locations (y/D_{in}), the x-component of velocity becomes negative. The reason is that as the flow passes through the first obstacle, large vortexes are formed behind the first obstacle (Figure 5(a)). The presence of such vortexes causes the establishment of the flow in most directions; therefore, the x- and y-components of velocity have negative values. As shown in Figure 12, the presence of a vortex with high α reduced the available space for the fluid to pass, thus increasing the velocity of the fluid above the first obstacle (α is defined in the Figure 10).

Figure 13 shows pressure profile for $x/D = 3.2$ as a function of Reynolds numbers for water-Al_2O_3(2%) nanofluid. The exact location of the section $x/D = 3.2$ is shown in Figure 6. D_{in} is the diameter of the input channel and the y-axis is shown in Figure 1. As shown in Figure 13, changes in pressure along the width of the channel are small. For the Reynolds number 300, the difference of the minimum and maximum pressures is about 6%. Also, for the Reynolds number 25, the difference of the minimum and maximum pressure is about 3%. This is because there is a small flow along the channel width; so, according to the momentum equation, changes in pressure will be small. The small flow along the channel width is also mainly due to the vortexes formed behind the first obstacle (Figure 5(a)). By raising the Reynolds number, the pressure drop of the system increases. For higher Reynolds numbers, this increase in pressure drop is more. For example, by increasing the Reynolds number from 2 to 5 (i.e., double and half of the Reynolds number), the pressure drop of the system is increased from 21 Pa to 52.7 Pa (i.e., double and half). However, by raising the Reynolds number from 100 to 200 (i.e., doubling the Reynolds number), the pressure drop of the system is increased from 2141 Pa to 5953 Pa (i.e., the pressure drop becomes about 2.8 times). Therefore, the system pressure drop will be better for low Reynolds numbers.

Figure 14 shows temperature profile for $x/D = 3.2$ for water-Al_2O_3 nanofluid as a function of volume fractions. The exact location of the section $x/D = 3.2$ is shown in Figure 6. D_{in} is the diameter of the inlet channel and the y-axis is shown in Figure 1. As shown, the change in nanofluid volume fraction has no effect on temperature profile. The maximum temperature in the curve is 300.3 K, which is related to the channel wall.

Figure 15 shows profile of x-component of velocity (m/s) for $x/D = 3.2$ for water-Al_2O_3 nanofluid with as a function of volume fraction. The exact location of the section $x/D = 3.2$ is shown in Figure 6. D_{in}

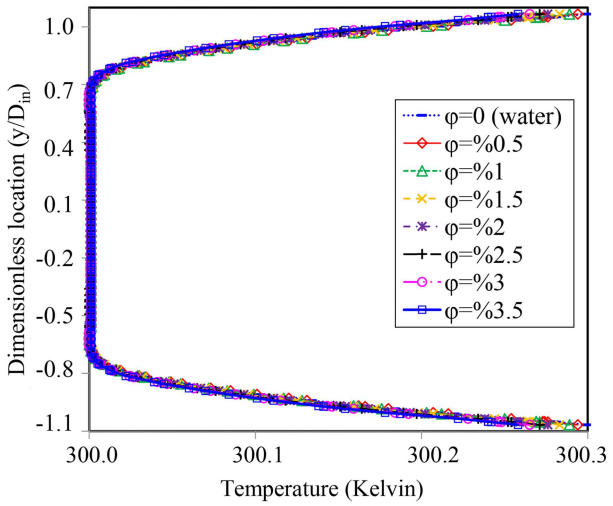

Figure 14. Temperature profile for $x/D_{in} = 3.2$ for water-Al_2O_3 nanofluid as a function of volume fraction. The exact location of the section $x/D = 3.2$ is shown in Figure 6. D_{in} is the diameter of the input channel and the y-axis is shown in Figure 1.

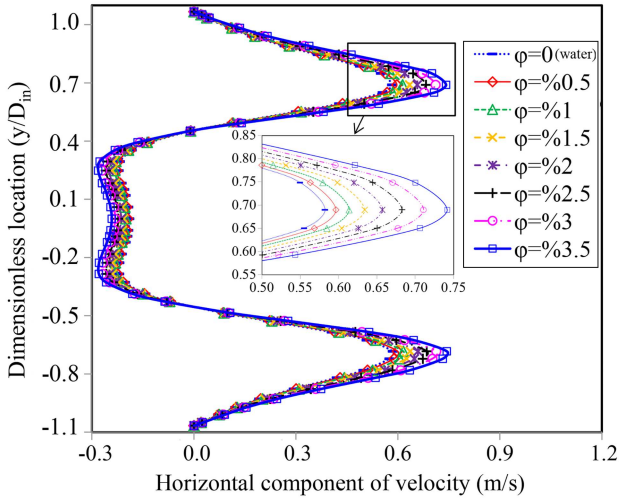

Figure 15. Profile of x-component of velocity (m/s) for $x/D = 3.2$ for water-Al_2O_3 nanofluid as a function of volume fractions. The exact location of the section $x/D = 3.2$ is shown in Figure 6. D_{in} is the diameter of the input channel and the y-axis is shown in Figure 1.

is the diameter of the input channel and the y-axis is shown in Figure 1. As shown, the volume fraction of the nanofluid has little effect on the velocity profile of the fluid. As can be seen in Figure 15, each of the velocity curves has two maximum velocity points. These points correspond approximately to $y/D_{in} = -0.7$ and $y/D_{in} = 0.7$.

According to Eq. (3), the Reynolds number is defined as $Re_{nf} = \frac{\rho_{nf}\bar{U}D}{\mu_{nf}}$. $\bar{U}$ is the inlet velocity of the system. As can be seen in Figure 15, the Reynolds number is considered equal to 100 for all curves. On the other hand, for each volume fraction,

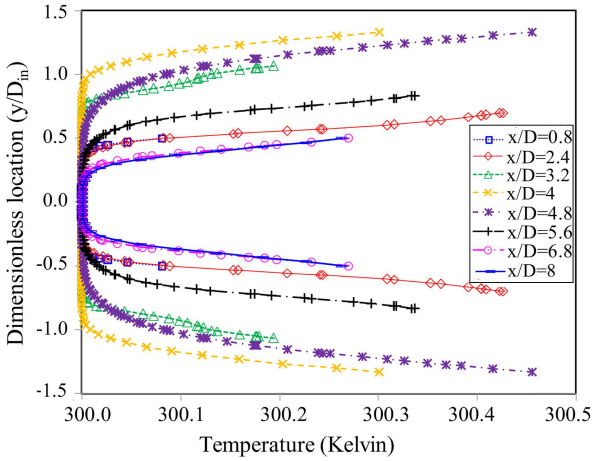

Figure 16. Temperature profile at different sections from the beginning to the end of the problem geometry for water-Al_2O_3(2%) nanofluid at the Reynolds number 200. The exact location of the sections is shown in Figure 6. D_{in} is the diameter of the input channel and the y-axis is shown in Figure 1.

the density and viscosity of nanofluid are calculated by Eq. (2). Therefore, for each volume fraction, the value $\bar{U}$ can be calculated by Eq. (3). For example, for the nanofluid with the volume fraction of 3%, we have $\bar{U}_{\%3} = 1.21$ m/s. Also, for the nanofluid with the volume fraction of 1%, we have $\bar{U}_{\%1} = 1.045$ m/s. Therefore, by increasing the nanofluid volume fraction, the inlet velocity of the system is raised. As a result, the velocity magnitude will increase in all sections.

According to Eq. (3), the Reynolds number is defined as $Re_{nf} = \frac{\rho_{nf}\bar{U}D}{\mu_{nf}}$. $\bar{U}$ is the inlet velocity of the system. In Figure 15, the Reynolds number is considered equal to 100 for all curves. On the other hand, for each volume fraction, the density and viscosity of nanofluid is calculated by Eq. (2). Therefore, for each volume fraction, the value $\bar{U}$ can be calculated by Eq. (3). For example, for nanofluid with volume fraction of 3%, we have $\bar{U}_{\%3} = 1.21$ m/s. Also, for nanofluid with volume fraction of 1%, we have $\bar{U}_{\%1} = 1.045$ m/s. Therefore, by increasing nanofluid volume fraction, the inlet velocity of the system increases. As a result, the velocity magnitude will increase in all sections.

Figure 16 shows temperature profile at different sections from the beginning to the end of the problem geometry for water-Al_2O_3(2%) nanofluid and the Reynolds number 200. The exact location of the sections is shown in Figure 6. D_{in} is the diameter of the input channel and the y-axis is shown in Figure 1. As shown in Figure 16, the temperature profile at sections $x/D = 3.2$, $x/D = 4$, and $x/D = 4.8$ is almost constant for $-0.6 < y/D_{in} < 0.6$. At other sections, there are constant temperature ranges, and these three sections have larger constant temperature ranges. This is due to the formation of two vortexes after the first

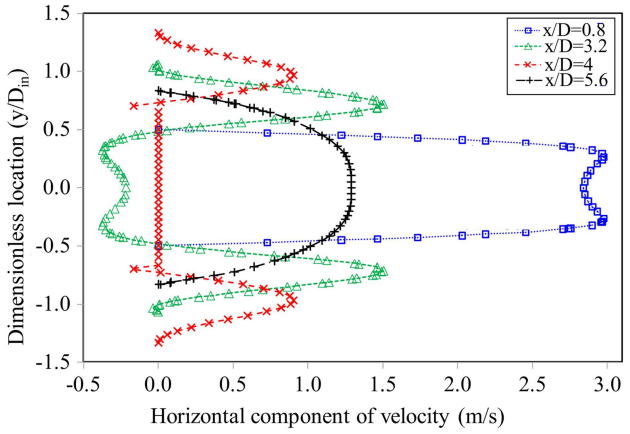

Figure 17. Profile of x-component of velocity (m/s) at different sections of the problem geometry for water-Al_2O_3(2%) nanofluid at the Reynolds number 200. The exact location of the sections is shown in Figure 6. D_{in} is the diameter of the input channel and the y-axis is shown in Figure 1.

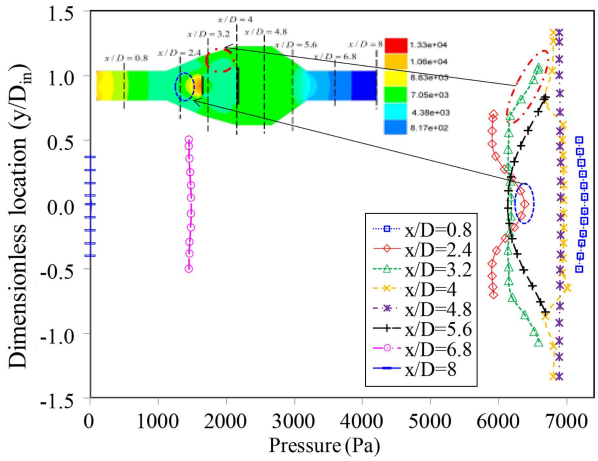

Figure 18. Pressure profile at different sections of the problem geometry for water-Al_2O_3(2%) nanofluid at the Reynolds number 200. D_{in} is the diameter of the input channel and the y-axis is shown in Figure 1.

obstacle and two vortexes after the second one. The inlet temperature of the fluid is 300 K and the walls have a thermal boundary condition of constant heat flux. Therefore, it can be said that as the fluid flow approaches the wall (in other words, the velocity of the fluid near the wall increases), the wall temperature is decreased. This is because the main fluid flow (at the temperature of 300 K) approaches the wall like a cold flow, reducing the wall temperature.

Figure 17 shows profile of x-component of velocity (m/s) at different sections of the problem geometry for water-Al_2O_3(2%) nanofluid at the Reynolds number of 200. In problem geometry, there are two obstacles. At the location of the obstacles, the flow is divided into two parts, half of which passes from the top of the obstacle and the other from the bottom of it (Figure 5(b)). Therefore, after the obstacle, we will have two flows, each of which has a maximum value. For this reason, as shown in Figure 17, there are two maximum velocities for $x/D_{in} = 3.2$ and $x/D_{in} = 4$. After the second obstacle, the flows passing through the top and bottom of the obstacle are combined to form a single flow (Figure 5(b)). For this reason, as shown in Figure 17, for $x/D_{in} = 5.6$, there is only one maximum velocity because there is only a flow there.

Figure 18 shows pressure profile at different sections of the problem geometry for water-Al_2O_3(2%) nanofluid at the Reynolds number of 200. As shown in Figure 18, for $x/D_{in} = 2.4$, the fluid pressure is the maximum in the center of the tube (the exact location of the section $x/D_{in} = 2.4$ is shown in Figure 18). The reason is that the section $x/D_{in} = 2.4$ is close to the first obstacle and at the location of the first obstacle, where the flow hits the obstacle, a stagnation point is formed on the obstacle; therefore, the pressure on the obstacle is increased. This increase of pressure is clearly shown in Figure 18. Now, because the section $x/D_{in} = 2.4$ is close to the location of the first obstacle, it senses the increase in pressure caused by the stagnation point; therefore, the pressure in the central points of the channel is increased. As shown in Figure 18, in the input and output channel (such as sections $x/D_{in} = 0.8$, $x/D_{in} = 6.8$, and $x/D_{in} = 8$), due to the lack of flow along the diameter of the tube, the pressure change along the diameter is very small. Also, at the sections with flow along the channel diameter (such as $x/D_{in} = 2.4$ and $x/D_{in} = 3.2$), the fluid pressure changes.

5. Conclusion

The results, thus, showed that the fluid velocity at the location of the first obstacle (and slightly before and after it) was almost the same; even when the flow reached the second obstacle, the flow velocity was decreased, which reduced the pressure drop in the proposed geometry. The results, therefore, showed that for the Reynolds number 50, increasing the temperature of the fluid in the geometry proposed in this study was 52% more than that of a simple tube under the same operating conditions. Also, for the Reynolds number 50, the pressure drop of the geometry proposed in this study was 24% less than that of a simple tube under the same operating conditions. It was also found that by increasing fluid velocity near the walls, the local Nusselt number was raised. The results also showed that the change in the volume fraction of nanoparticles had a small effect on the Nusselt number, so that the average Nusselt number in the volume fraction of 3.5% was about 4% higher than that in 0.5%. In addition, by increasing the Reynolds number, the average pressure of the fluid at different sections of the geometry was increased. The results indicated the average Nusselt

number for $Re = 100$ is %128 more than the Nusselt number of $Re = 2$. Also, changing the volume fraction of the nanofluid had a slight effect on velocity profile and no effect on the temperature profile.

Nomenclature

c	Specific heat capacity
d	Channel diameter
h	Convection heat transfer coefficient
k	Thermal conductivity
T^*	Dimensionless temperature (Eq. (9))
P^*	Dimensionless pressure (Eq. (10))
Re	Reynolds number
Nu	Nusselt number
ρ	Density
μ	Viscosity
φ	Volume fraction of nanoparticles

Subscriptions

n_f	Nanofluid
p	Nanoparticles
b_f	Base fluid

References

1. Askari, N. and Taheri, M.H. "Numerical investigation of a MHD natural convection heat transfer flow in a square enclosure with two heaters on the bottom wall", *Karafan Research Journal of Technical and Vocational University of Iran*, **17**(1), pp. 101–121 (2020). DOI: 10.48301/kssa.2020.112759
2. Outokesh, M., Moosavi-Ajarostaghi, S.S., Bozorgzadeh, A., et al. "Numerical evaluation of the effect of utilizing twisted tape with curved profile as a turbulator on heat transfer enhancement in a pipe", *J. Therm. Anal. Calorim.*, **140**, pp. 1537–1553 (2020). DOI: 10.1007/s10973-020-09336-0
3. Nakhchi, M.E. "Experimental optimization of geometrical parameters on heat transfer and pressure drop inside sinusoidal wavy channels", *Thermal Science and Engineering Progress*, **9**, pp. 121–131 (2019). DOI: 10.1016/j.tsep.2018.11.006
4. Shamsi, M.R., Akbari, O.A., Marzban, A., et al. "Increasing heat transfer of non-Newtonian nanofluid in rectangular microchannel with triangular ribs", *Physica E*, **93**, pp. 167–178 (2017). DOI: 10.1016/j.physe.2017.06.015
5. Ali Akbari, O., Toghraie, D., Karimipour, A., et al. "The effect of velocity and dimension of solid nanoparticles on heat transfer in non-Newtonian nanofluid", *Physica E: Low-dimensional Systems and Nanostructures*, **86**, pp. 68–75 (2017). DOI: 10.1016/j.physe.2016.10.013
6. Masoumnezhad, M., Kazemi, M.A., Askari, N., et al. "Semi-analytical solution of unsteady newtonian fluid flow and heat transfer between two oscillation plate under the influence of a magnetic field", *Karafan*, **18**(1), pp. 35–62 (2021). DOI: 10.48301/kssa.2021.131037
7. Mousa, M.H., Miljkovic, N., and Nawaz, K. "Review of heat transfer enhancement techniques for single phase flows", *Renewable and Sustainable Energy Reviews*, **137**, p. 110566 (2021). DOI: 10.1016/j.rser.2020.110566
8. Khetib, Y., Alahmadi, A., Alzaed, A., et al. "Application of cylindrical fin to improve heat transfer rate in micro heat exchangers containing nanofluid under magnetic field", *Processes*, **9**, p. 1278 (2021). DOI: 10.3390/pr9081278
9. Kia, S.M., Khanmohammadi, S., and Jahangiri, A. "Experimental and numerical investigation on heat transfer and pressure drop of SiO_2 and Al_2O_3 oil-based nanofluid characteristics through the different helical tubes under constant heat fluxes", *International Journal of Thermal Sciences*, **185**, p. 108082 (2023). DOI: 10.1016/j.ijthermalsci.2022.108082
10. Akbarzadeh, S. and Valipour, M.S. "Experimental study on the heat transfer enhancement in helically corrugated tubes under the non-uniform heat flux", *J. Therm. Anal. Calorim.*, **140**, pp. 1611–1623 (2020). DOI: 10.1007/s10973-020-09385-5
11. Nguyen, Q., Bahrami, D., Kalbasi, R., et al. "Nanofluid flow through microchannel with a triangular corrugated wall: Heat transfer enhancement against entropy generation intensification", *Mathematical Methods in the Applied Sciences*, **33**, pp. 1–14 (2020). DOI: 10.1002/mma.6705
12. Pahlevaninejad, N., Rahimi, M., and Gorzin, M. "Thermal and hydrodynamic analysis of non-Newtonian nanofluid in wavy microchannel", *J. Therm. Anal. Calorim.*, **143**, pp. 811–825 (2021). DOI: 10.1007/s10973-019-09229-x
13. Rahmati, A.R. and Derikvand, M. "Numerical study of non-Newtonian nano-fluid in a micro-channel with adding slip velocity and porous blocks", *International Communications in Heat and Mass Transfer*, **118**, p. 104843 (2020). DOI: 10.1016/j.icheatmasstransfer.2020.104843
14. Abdelmalek, Z., D'Orazio, A., and Karimipour, A. "The effect of nanoparticle shape and microchannel geometry on fluid flow and heat transfer in a porous microchannel", *Symmetry*, **12**(4), p. 591 (2020). DOI: 10.3390/sym12040591
15. Miansari, M., Aghajani, H., Zarringhalam, M., et al. "Numerical study on the effects of geometrical parameters and Reynolds number on the heat transfer behavior of carboxy-methyl cellulose/CuO non-Newtonian nanofluid inside a rectangular microchannel", *J. Therm. Anal. Calorim.*, **144**, pp. 179–187 (2021). DOI: 10.1007/s10973-020-09447-8

16. Cheng, X., Li, Z.R., Wan, H.N., et al. "Experimental investigation on convective heat transfer of hydrocarbon fuel in transverse corrugated tubes", *International Journal of Heat and Mass Transfer*, **201**(1), p. 123586 (2023).
DOI: 10.1016/j.ijheatmasstransfer.2022.123586

17. Zhang, L., Yan, X., Zhang, Y., et al. "Heat transfer enhancement by streamlined winglet pair vortex generators for helical channel with rectangular cross section", *Chemical Engineering and Processing - Process Intensification*, **147**, p. 107788 (2020).
DOI: 10.1016/j.cep.2019.107788

18. Borah, A., Boruah, M.P., and Pati, S. "Conjugate heat transfer in a duct using nanofluid by two-phase Eulerian-Lagrangian method: Effect of non-uniform heating", *Powder Technology*, **346**, pp. 180–192 (2019).
DOI: 10.1016/j.powtec.2019.01.059

19. Borah, A. and Pati, S. "Influence of non-uniform asymmetric heating on conjugate heat transfer in a rectangular mini channel using nanofluid by two-phase Eulerian-Lagrangian method", *Powder Technology*, **381**, pp. 164–180 (2021).
DOI: 10.1016/j.powtec.2020.12.037

20. Faizan, M., Pati, S., and Randive, P.R. "Implication of geometrical configuration on heat transfer enhancement in converging minichannel using nanofluid by two phase mixture model: A numerical analysis", *Proceedings of the Institution of Mechanical Engineers, Part E: Journal of Process Mechanical Engineering*, **235**(2), pp. 1–12 (2020).
DOI: 10.1177/0954408920964694

21. Bhowmick, D., Randive, P.R., and Pati, S. "Implication of corrugation profile on thermo-hydraulic characteristics of Cu-water nanofluid flow through partially filled porous channel", *International Communications in Heat and Mass Transfer*, **125**, p. 105329 (2021).
DOI: 10.1016/j.icheatmasstransfer.2021.105329

22. Mehta, S.K. and Pati, S. "Analysis of thermo-hydraulic characteristics for flow of MWCNT-Fe_3O_4/H_2O hybrid nanofluid through a wavy channel under magnetic field", *Proceedings of the Institution of Mechanical Engineers Part E: Journal of Process Mechanical Engineering*, **238**(1), pp. 67–77 (2022).
DOI: 10.1177/09544089221094206

23. Faizan, Md., Pati, S., and Randive, P.R. "Effect of non-uniform heating on conjugate heat transfer performance for nanofluid flow in a converging duct by a two-phase Eulerian-Lagrangian method", *Proceedings of the Institution of Mechanical Engineers Part E: Journal of Process Mechanical Engineering*, **236**(2), pp. 414–424 (2022).
DOI: 10.1177/09544089211042951

24. Minea, A.A. "Uncertainties in modeling thermal conductivity of laminar forced convection heat transfer with water alumina nanofluids", *International Journal of Heat and Mass Transfer*, **68**, pp. 78–84 (2014).
DOI: 10.1016/j.ijheatmasstransfer.2013.09.018

25. Mukherjee, S., Jana, S., Mishra, P.C., et al. "Experimental investigation on thermo-physical properties and subcooled flow boiling performance of Al_2O_3/water nanofluids in a horizontal tube", *International Journal of Thermal Sciences*, **159**, p. 106581 (2021).
DOI: 10.1016/j.ijthermalsci.2020.106581

26. Zeinali-Heris, S., Nasr-Esfahany, M., and Etemad, Gh. "Experimental investigation of convective heat transfer of Al_2O_3/water nanofluid in circular tube", *International Journal of Heat and Fluid Flow*, **28**(2), pp. 203–210 (2007).
DOI: 10.1016/j.ijheatfluidflow.2006.05.001

27. Tang, W., Zhu, S., Jiang, D., et al. "Channel innovations for inertial microfluidics", *Lab on a Chip*, **20**, pp. 3485–3502 (2020).
DOI: 10.1039/D0LC00714E

28. Mehta, S.K. and Pati, S. "Analysis of thermo-hydraulic performance and entropy generation characteristics for laminar flow through triangular corrugated channel", *J. Therm. Anal. Calorim.*, **136**, pp. 49–62 (2019).
DOI: 10.1007/s10973-018-7969-1

29. Kim, D., Kwon, Y., Cho, Y., et al. "Convective heat transfer characteristics of nanofluids under laminar and turbulent flow conditions", *Current Applied Physics*, **9**, pp. e119–e123 (2009).
DOI: 10.1016/j.cap.2008.12.047

30. Chandrasekar, M., Suresh, S., and Chandra-Bose, A. "Experimental studies on heat transfer and friction factor characteristics of Al_2O_3/water nanofluid in a circular pipe under laminar flow with wire coil inserts", *Experimental Thermal and Fluid Science*, **34**, pp. 122–130 (2010).
DOI: 10.1016/j.expthermflusci.2009.10.001

Biography

Ahmad Bedram received his BSc degree in mechanical engineering (energy conversion) from Isfahan University of Technology in 2009. Also, he received his MSc and PhD degrees in mechanical engineering (energy conversion) from Sharif University of Technology in 2011 and 2015, respectively. He is an Assistant Professor at the Mechanical Engineering Department at Technical and Vocational University of Tehran, Iran. He has several published papers on symmetric and asymmetric droplet breakup in T-junction and similar geometries. Also, the flow pattern of micro and nano droplets is investigated in his papers. Currently, he is working on the heat transfer enhancement of nanofluids in the internal flows. The research method of his papers is computational fluid dynamic and Volume of Fluid (VOF) method for multiphase flows simulations.